Particle & Particle Systems Characterization
www.particle-journal.com

Composition-Controlled Laser-Induced Alloying of Colloidal Au–Cu Hetero Nanoparticles

*Daniel Kranz, Patrick Bessel, Marina Rosebrock, Max Niemeyer, and Dirk Dorfs**

Due to their optical properties (localized surface plasmon resonance, LSPR), colloidally dispersed metal nanoparticles are well suited for selective heating by high-energy laser radiation above their melting point without being limited by the boiling point of the solvent, which represents an excellent complement to wet-chemical nanoparticle synthesis. By combining wet-chemical synthesis and postsynthesis laser treatment, the advantages of both methods can be used to specifically control the properties of nanoparticles. Especially in the colloidal synthesis of nanoalloys consisting of two or more metals with different redox potentials, wet-chemical synthesis quickly reaches its limits in terms of composition control and homogeneity. For this reason, the direct synthesis path is divided into two parts to take the strengths of both methods. After preparing Au–Cu hetero nanoparticles by wet-chemical synthesis, nanoalloys with previous adjusted composition can be formed by postsynthesis laser treatment. The formation of these nanoalloys can be followed by different characterization methods, such as transmission electron microscopy (TEM), where the fusion of both metal domains and the formation of spherical and homogeneous Au–Cu nanoparticles can be observed. Moreover, the alloy formation can be followed by different shifts of X-ray diffraction (XRD) reflections and LSPR maxima depending on the composition.

1. Introduction

Nanoparticles possess interesting new properties compared to bulk materials. For example, metallic nanoparticles show high absorption cross sections due to their plasmonic properties (localized surface plasmon resonance, LSPR), which make them well suitable for heating by high-energy light sources. This process is called plasmonic heating.[1,2] Due to their monochromatic light and their high point intensities, laser systems are well suited as light sources for such processes. Heating in colloidal solution is of particular interest since this is only possible to a limited extent by conventional ways such as heating of the entire liquid phase due to the limitation of the achievable temperature by the boiling point of the solvent.[1,3] By absorbing a specific wavelength and simultaneous optical transparency of the surrounding medium, nanoparticles can be selectively heated to temperatures well above their melting point, while the surrounding medium remains almost at room temperature.[4] In general, laser processes involving colloidal particles are divided into various subgroups under the generic term laser synthesis and processing of colloids (LSPC), which differ primarily in the starting material (substrate, macro- or nanoparticles), the focusing of the laser beam and the laser intensity.[5] In so-called laser ablation in liquids (LAL) and laser fragmentation in liquids (LFL) processes, nanoparticles are synthesized by vaporization and fragmentation from target substrates or macro particles at high point intensities. In contrast, milder conditions are used in laser melting in liquids (LML) processes, whereby only melting of the particles is to be achieved.[5,6] In this way, for example, it is possible to reshape rod-shaped gold particles into spherical nanoparticles.[7] Furthermore, it is possible to influence the crystal structure and to induce phase transitions.[8,9]

In addition to monometallic compounds, intermetallic nanoparticles such as nanoparticle alloys exhibit new properties, which make them very interesting for applications in catalysis,[10] electronics,[11] sensing[12] as well as for biomedical applications.[13] Nanoparticle alloys can be synthesized by various methods, such as chemical reduction, seed-mediated diffusion, and electrochemical deposition. The mainly used method is wet-chemical co-reduction, in which two metal precursors are reduced simultaneously resulting in an alloy.[14–16] By adjusting the ratio of the metal precursors, different compositions can

D. Kranz, P. Bessel, M. Rosebrock, M. Niemeyer, D. Dorfs
Institute of Physical Chemistry and Electrochemistry
Leibniz University Hannover
30167 Hannover, Germany
E-mail: dirk.dorfs@pci.uni-hannover.de

D. Kranz, P. Bessel, M. Rosebrock, M. Niemeyer, D. Dorfs
Laboratory of Nano and Quantum Engineering
Leibniz University Hannover
30167 Hannover, Germany

M. Rosebrock, D. Dorfs
Cluster of Excellence PhoenixD (Photonics, Optics, and Engineering – Innovation Across Disciplines)
Leibniz University Hannover
30167 Hannover, Germany

The ORCID identification number(s) for the author(s) of this article can be found under https://doi.org/10.1002/ppsc.202300021

© 2023 The Authors. Particle & Particle Systems Characterization published by Wiley-VCH GmbH. This is an open access article under the terms of the Creative Commons Attribution-NonCommercial License, which permits use, distribution and reproduction in any medium, provided the original work is properly cited and is not used for commercial purposes.

DOI: 10.1002/ppsc.202300021

be obtained.[15,17] To obtain a homogeneous alloy, similar redox potentials are required, which is often difficult to achieve.[14,15,18] Prunier et al. therefore compared the formation of an Au–Cu alloy via two different methods. They observed that coreduction of the Au and Cu precursor in a wet-chemical coreduction process tends to result in an inhomogeneous compound with monometallic domains. Furthermore, compositional control proved to be difficult. In contrast by using a pulsed laser deposition (PLD) process, homogeneous compounds with a targeted composition could be obtained.[18] In the meantime, laser processes have been added to the list of possible synthesis methods for nanoparticle alloys. In general, commonly used laser processes for the synthesis of nanoalloys are based on two approaches, the irradiation of alloy substrates with a target composition and the laser treatment of a mixture of monometallic colloids or metal salts in solution.[19,20–22] It is also possible to form alloy nanoparticles by thermal diffusion of presynthesized hetero nanoparticles. The possibility of such a procedure was already published by Gonzáles-Rubio et al. who obtained Au–Ag alloys starting from colloidal Au–Ag core–shell nanorods. They further showed that the degree of alloying can be controlled by appropriate laser parameters (laser fluence, number of laser pulses).[23] The control of the degree of alloying by thermal diffusion has also been shown by van der Hoeven et al. In contrast to the previously mentioned laser procedure, they heated Au–Ag core–shell nanoparticles inside a transmission electron microscope (TEM) by using a heated sample holder to observe the alloy formation in situ by energy dispersive X-ray spectroscopy (EDX) as a function of temperature and composition.[24]

In this work, we continue the previous mentioned pioneer work on this topic by the investigation of the composition-controlled laser-induced alloying of colloidally dispersed Au–Cu hetero nanoparticles. Apart from ablation/fragmentation laser processes and the above-mentioned control of the degree of alloying, especially the composition-control of nanoalloys starting from well-defined colloidal hetero nanoparticles by a LML process has not been well studied. However, this process offers great potential due the combination of the strengths of wet-chemical synthesis and selective laser treatment of colloidal nanoparticles. For this purpose, Au–Cu hetero nanoparticles with different gold to copper ratios shall be prepared in the first step. By wet-chemical synthesis the homogeneous growth of the copper domains on gold nanoparticles can be controlled very well by varying the amount of copper precursor. Alloy formation shall then be achieved by laser treatment of the colloidal solution. Due to the selective heating and melting process of the Au–Cu hetero nanoparticles, fusion of the metal domains occurs. By heating above the melting point, homogeneous mixing of the metal atoms will be achieved, resulting in the formation of a nanoalloy after resolidification. Due to the isochoric melting process, the composition of the individual particles does not change compared to the initial hetero nanoparticles. Thus, the composition (gold to copper ratio) of the laser-induced nanoalloys can be previously adjusted and controlled by wet chemical synthesis, which opens the door for controllable alloying processes of a variety of further metal systems such as Au–Ag,[21–23,25] Ag–Bi,[26] Au–Fe,[20] Au–Zn,[27] Fe–Pt,[28] and Ag–Pt,[29] whose alloy formation could already be observed by LAL and LFL methods. In principle, the implementation of this method is conceivable for all alloy-forming metal systems as long as they exhibit suitable absorption properties in the range of the laser wavelength.

2. Results and Discussion

Au–Cu hetero nanoparticles were synthesized using a slightly modified procedure described by Jia et al. (see Section 4 for details). The amount of copper precursor was varied to obtain Au–Cu hetero nanoparticles with different sized copper domains on gold nanoparticles. In addition, copper nanoparticles were prepared using the same procedure without adding gold particles. All particles are illustrated in **Figure 1**. The gold nanoparticles have an average particle size of (39.9 ± 3.5) nm. The sizes of the copper domains are approximately (13.9 ± 3.2) nm (3:1 Au–Cu-ratio) nm, (26.7 ± 6.0) nm (1:1 Au–Cu-ratio) and (35.1 ± 12.1) nm (1:3 Au–Cu-ratio). These sizes are difficult to evaluate by TEM images due to their anisotropic shape. To get comparable particle sizes, the thickest part of the copper domain was determined. The synthesized copper nanoparticles have an average particle size of (56.4 ± 7.4) nm (see Figures S1-S5 in the Supporting Information for details). To consider the laser-induced heating process of Au–Cu hetero nanoparticles more in detail, the absorption efficiencies of gold and copper nanoparticles were calculated using Mie theory (see Figure S6 in the Supporting Information for details). The calculations show that both the gold and the copper nanoparticles exhibit high absorption efficiencies in the range of the laser wavelength of 532 nm. According to these results, both metal particles are well suited for laser-induced heating experiments. In the particle size range considered here (<50 nm), the absorption efficiency of gold is about twice as high as the absorption efficiency of copper. For this reason, it can be assumed that the gold domain can be heated to higher temperatures and thus primarily induces the melting or alloying process. The Au–Cu hetero nanoparticles were then irradiated with the second harmonic of a nanosecond Nd:YAG laser (532 nm, 20 mJ cm^{-2}, 10 laser pulses). Figure 1 illustrates the particles before (Figure 1A–F) and after the laser treatment (Figure 1G–J). After the laser treatment, all particles are spherical in shape (thermodynamically most favorite shape), which indicates a successful laser-induced melting and resolidification process. The fusion of the gold and copper domains leads to an increase in the entire particle size. The volume of the particles corresponds approximately to the summed volume of both metal domains before the laser treatment (Figures S1–S5, Supporting Information). A growth of the particles, as described in many reports on LML processes mostly due to (pre-)agglomeration, cannot be observed here.[8,30] This isochoric fusion is probably the result of a high colloidal stability as well as a low laser fluence and a low number of laser pulses.[31] The hetero structure of the Au–Cu hetero nanoparticles disappears after the laser treatment, indicating the formation of Au–Cu nanoalloys. In contrast, particles with different contrasts are still visible in the case of the simple mixture of gold and copper nanoparticles. To investigate if nanoalloys were formed, TEM energy dispersive X-ray spectroscopy (TEM-EDX) mappings of the Au–Cu hetero nanoparticles with an Au–Cu-ratio of 1:3 and of the mixture before and after the laser treatment were taken. Here, due to the expected equivalent behavior of all three Au–Cu hetero particle solutions, the particles with the largest copper domains were chosen for the TEM-EDX mapping

© 2023 The Authors. Particle & Particle Systems Characterization published by Wiley-VCH GmbH

15214117, 0, Downloaded from https://onlinelibrary.wiley.com/doi/10.1002/ppsc.202300021 by Cochrane Germany, Wiley Online Library on [13/07/2023]. See the Terms and Conditions (https://onlinelibrary.wiley.com/terms-and-conditions) on Wiley Online Library for rules of use; OA articles are governed by the applicable Creative Commons License

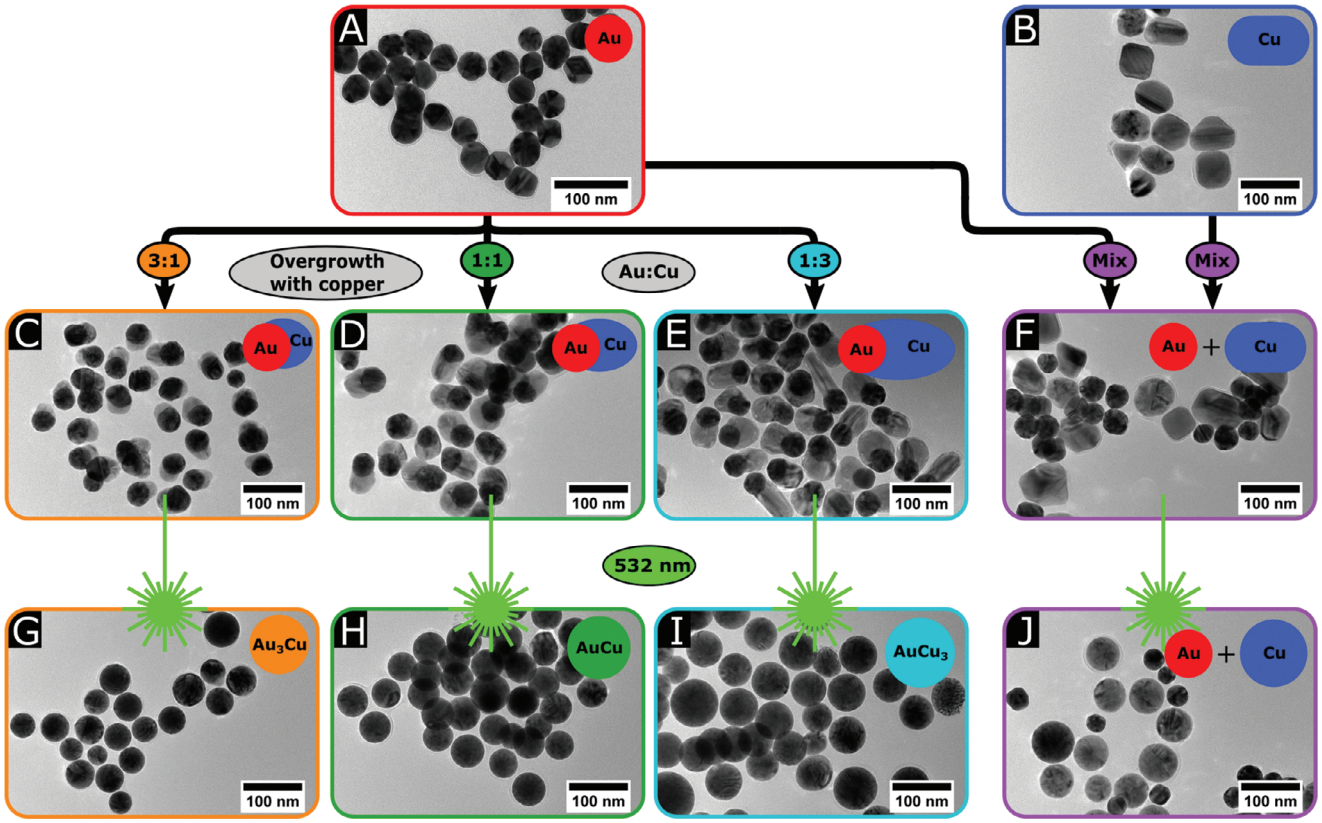

Figure 1. A–F) Laser-induced composition-controlled alloying of Au–Cu hybrid nanoparticles with different ratios of Au and Cu and comparison with a mixture of Au and Cu nanoparticles. G–J) After the laser treatment, the hetero particles were transformed into spherical alloy nanoparticles. In the case of a mixture, the Au and Cu nanoparticles were also reshaped into spherical particles but not alloyed during the heating process.

and the observation of the alloying process. In the TEM-EDX mappings, illustrated in **Figure 2**, the hetero nanoparticles show different colored and separated gold (red) and copper domains (blue) before the laser treatment (Figure 2A–H). After the irradiation process (Figure 2I–P), the gold and copper signals are homogeneous distributed over the entire particle volume, which in turn results from the formation of Au–Cu alloys without monometallic domains. The slightly blue background of the gold nanoparticles results from copper parts inside the TEM (interference radiation). In contrast, the mixture of gold and copper nanoparticles without direct particle contact to each other does not result in the formation of alloys, showing that a direct contact is required for the fusion of two metal domains in LML processes compared to different laser processes with higher laser fluences, like LFL processes. In addition to these results, reference experiments were also performed to investigate if also a one-step process of the synthesis solution would lead to equivalent results. For this purpose, colloidally dispersed gold nanoparticles, a copper(II) chloride solution and the wet-chemical synthesis mixture without the addition of reducing agents were laser-treated. In summary, no evidences of an alloying process were obtained, confirming the requirement of the two-step process consisting of wet-chemical synthesis and subsequent laser treatment (see Figure S7 in the Supporting Information for details).

The formation of Au–Cu nanoalloys were also investigated by X-ray diffraction (XRD). **Figure 3** illustrates XRD diffractograms of all three Au–Cu hetero particle solutions (Figure 3A–C) as well as the mixture of gold and copper nanoparticles (Figure 3D). Before the laser treatment, all reflections can be assigned to either elemental gold (38.2° 2θ, 44.4° 2θ, 64.7° 2θ, 77.7° 2θ) or copper (43.5° 2θ, 50.6° 2θ, 74.3° 2θ). After laser treatment, in the case of the mixture of gold and copper particles (Figure 3D), there is only a slight change in the intensities of the reflections which results from the reshaping of the particles due to the melting process. In the case of the hetero nanoparticles (Figure 3A–C), the intensity of the reflections which can be assigned to gold and copper decreases, while new reflections appear which can be assigned to Au–Cu alloys (Au_3Cu: 39.8° 2θ, 46.0° 2θ, 67.2° 2θ; AuCu: 40.7° 2θ, 47.2° 2θ, 69.1° 2θ; $AuCu_3$: 41.9° 2θ, 48.6° 2θ, 71.3° 2θ). The yield of nanoalloys decreases with increasing copper domain size (Figure 3A–C), which could be related to the optical density and the energy profile of the laser beam. On the one hand, an increase in particle size results in an increase in shadow effects. On the other hand, more material must be heated. Since the heating of the hetero nanoparticles occurs primarily via the gold domain, more energy is required for the entire alloying process. Due to the gaussian energy profile of the laser beam, the nanoparticles must be localized closer to the center of the beam. As a result, less particles in total can be heated to temperatures above the melting point per laser pulse and the probability of nonheated hetero particles and intermediates increases. The position of these reflections varies depending on the Au–Cu ratio and are located closer

© 2023 The Authors. Particle & Particle Systems Characterization published by Wiley-VCH GmbH

15214117, 0, Downloaded from https://onlinelibrary.wiley.com/doi/10.1002/ppsc.202300021 by Cochrane Germany, Wiley Online Library on [13/07/2023]. See the Terms and Conditions (https://onlinelibrary.wiley.com/terms-and-conditions) on Wiley Online Library for rules of use; OA articles are governed by the applicable Creative Commons License

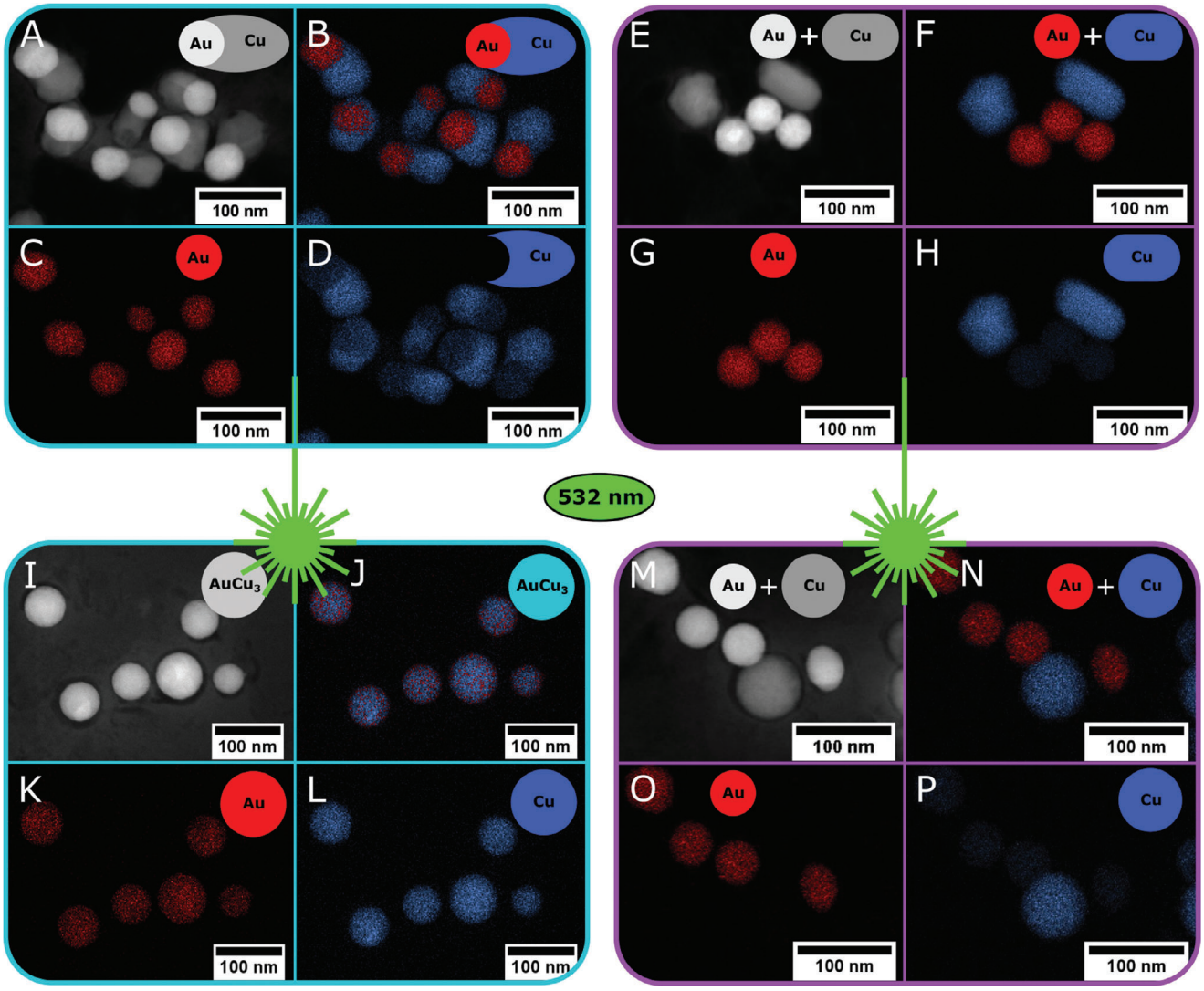

Figure 2. A–H) TEM-EDX mappings before and I–P) after the laser treatment of Au–Cu hetero nanoparticles (Au:Cu – 1:3) and a mixture of gold and copper nanoparticles. In contrast to the mixture, gold and copper domains fused together and the correspond signals (Au: red, Cu: blue) are homogeneous distributed after the laser treatment in the case of the hetero particles. The slightly blue background of the gold nanoparticles results from copper parts inside the TEM (interference radiation).

to the reflections of elemental gold or copper. These observations are consistent with the existing literature. By laser ablation of Au–Cu nanoalloys on a TiO_2 substrate with increasing gold content, Hong et al. also observed a shift of the reflection characteristic for Cu towards the value for Au. The higher the gold content, the closer to the characteristic gold position.[32] The higher the copper content in the hetero particles and finally in the nanoalloy, the further the XRD reflections of the alloys shift away from the values of gold and approach the typical values for copper. This results from the increasing occupation of the gold lattice structure by copper atoms. The position of the reflection can be used to determine the respective lattice constant (see Figure S8 in the Supporting Information for details). The lattice parameter can be used to determine the percentage composition. According to Vegard's law, which describes the dependence of the lattice constant of an alloy on its composition, the composition of the nanoalloys was determined after the laser treatment.[33] The alloyed Au–Cu hetero particles with a gold to copper ratio of 3:1 (Au:Cu) thus contain 68.7% Au and 31.3% Cu. The alloy therefore contains a slightly higher copper content than expected. In contrast, the alloyed hetero nanoparticles with a gold to copper ratio of 1:1 and 1:3 (Au:Cu) show very good agreements with the gold to copper ratio used during the wet-chemical synthesis, with 49.2% Au and 50.8% Cu, and 25.1% Au and 74.9% Cu respectively (see Table S1 in the Supporting Information). The reflections of the nanoalloys exhibit a higher full width at half maximum. Since the width of the Scherrer reflections correlates directly with the size of the crystalline domains, this could indicate a decrease in the domain size after the laser treatment. On the one hand an increase of the width of the reflections and a decrease of the crystalline domain size therefore probably results from an increase of the polycrystallinity of the nanoparticles during the laser treatment and after

 © 2023 The Authors. Particle & Particle Systems Characterization published by Wiley-VCH GmbH

15214117, 0, Downloaded from https://onlinelibrary.wiley.com/doi/10.1002/ppsc.202300021 by Cochrane Germany, Wiley Online Library on [13/07/2023]. See the Terms and Conditions (https://onlinelibrary.wiley.com/terms-and-conditions) on Wiley Online Library for rules of use; OA articles are governed by the applicable Creative Commons License

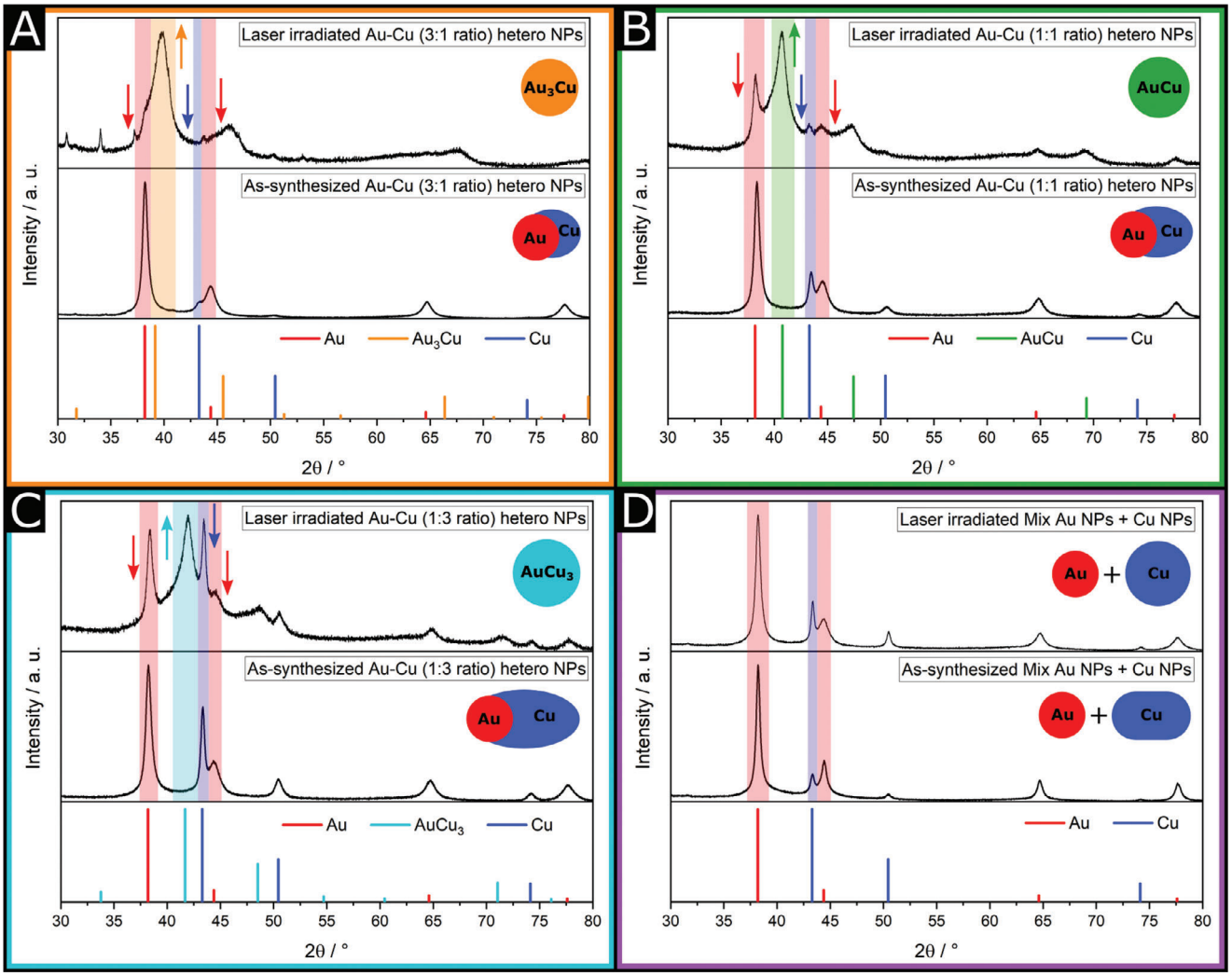

Figure 3. A–C) X-ray diffraction of the laser-induced, composition-controlled alloying of Au–Cu hetero nanoparticles. The composition of the alloy can be controlled by the gold to copper ratio of the hetero particles. D) In the case of a mixture of gold and copper nanoparticles, no alloy is formed.

the resolidification process. Additionally, this could also be the result of a mixture of different, not exactly stoichiometric alloy phases. Since a certain size distribution can be expected both in the synthesis of the gold nanoparticles and in the growth of the copper domains, a slight deviation of individual particles from the ideal composition is well in line with expectations. This is also supported by the fact that the gold–copper system is a fully miscible system and can be confirmed by TEM. Here, not all gold particles are exactly uniformly overgrown by copper domains. Additionally, it is also possible that the metal domains are not yet fully but only partially fused, which would be expected especially with increasing copper domain size and would also result in a slight deviation from the ideal stoichiometric composition. Nevertheless, when comparing the previously determined percent compositions of the laser-treated nanoalloys by XRD, it clearly shows that they agree well with the ratios of gold to copper used during the wet-chemical synthesis.

In addition to the crystal structure, the particles were also optically characterized before and after the laser treatment, illustrated in **Figure 4**. Initially, two maxima in the absorbance are observed in all hetero particle solutions (Figure 4A–C) as well as in the case of the mixture of gold and copper nanoparticles (Figure 4D). These result from the localized surface plasmon resonance (LSPR) of the metal domains. The LSPR bands of the hetero particles at 540 nm can be assigned to gold and the LSPR band at 585 nm can be assigned to copper. Both are bathochromically shifted compared to the bands of the pure metal nanoparticles in the mixed solution. This can be expected due to the direct particle contact and resulting change of the dielectric environment. During the laser treatment, the absorbance of the LSPR bands of all investigated particle solutions decreases, which results from the reshaping of the particles because of the melting process. In addition, after the laser treatment of the hetero nanoparticles, a new band appears between the positions of the LSPR bands of gold and copper, while the absorbance of the gold and copper LSPR decreases with an increasing number of laser pulses. This indicates a conversion of the monometallic domains into an alloy structure. The position of this band depends on the Au–Cu ratio,

© 2023 The Authors. Particle & Particle Systems Characterization published by Wiley-VCH GmbH

15214117, 0, Downloaded from https://onlinelibrary.wiley.com/doi/10.1002/ppsc.202300021 by Cochrane Germany, Wiley Online Library on [13/07/2023]. See the Terms and Conditions (https://onlinelibrary.wiley.com/terms-and-conditions) on Wiley Online Library for rules of use; OA articles are governed by the applicable Creative Commons License

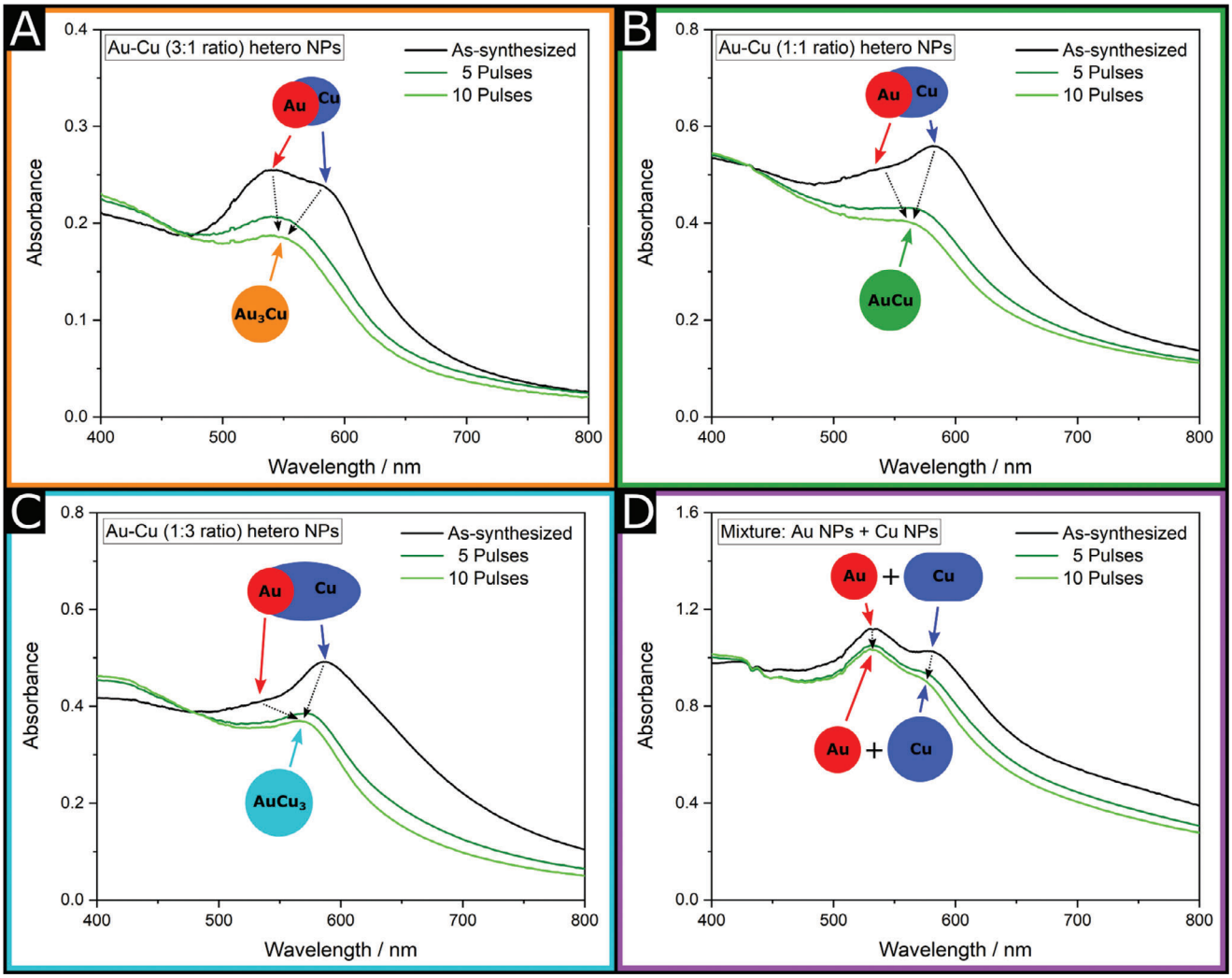

Figure 4. UV–vis spectra of the composition controlled alloying of Au–Cu hybrid nanoparticles during laser irradiation. After the laser-induced heating process, the typical bands for the localized surface plasmon resonances (LSPRs) of Au and Cu were transformed into one single band between both positions. A–C) The position of the new band is dependent on the composition of the nanoalloy. D) In the case of the mixture of gold and copper nanoparticles without direct particle contact, the LSPR bands of gold and copper are still visible and no additional appears.

like the position of the XRD reflections (Figure 3A–C), which is consistent with the existing literature. Kuladeep et al. observed this dependence of the LSPR band of nanoalloys on the composition also for Au–Ag alloys. They show a linear shift of the position of the Au LSPR to the Ag LSPR with increasing silver content.[21] Based on the position of the LSPR Maximum of the nanoalloy compared to the position of the Au and Cu LSPR maxima, the composition can also be determined, equivalent to the determinations based on the positions of the XRD reflections and lattice constants. In this case, a gold to copper ratio of 3:1 (Au:Cu) results in a percentage composition of 70.8% Au and 29.2% Cu. Similar to the determination of the composition via the lattice constants, a slightly higher copper content than expected can be observed here. With gold to copper ratios of 1:1 and 1:3 (Au:Cu), percentage compositions of 47.9% Au and 52.1% Cu, and 27.1% Au and 72.9% Cu respectively could be determined which are well in line with the gold to copper ratios used for the wet-chemical synthesis of the hetero particles and the values determined via the lattice constants (see Table S2 in the Supporting Information for details). In contrast to the shifting of the LSPR Maxima in the case of the hetero particles, in the case of the mixture of gold and copper nanoparticles (Figure 4D), the LSPR bands of both metals are preserved. To investigate if an accumulation of laser pulses is required or if this alloying process is a single-pulse process, additional single pulse experiments, illustrated in **Figure 5**, were performed. In all cases (Figure 5A–C), the formation of nanoalloys occur already after one single pulse (Figure 5D–F, some alloyed Au–Cu particles are highlighted in red circles), which demonstrates that the melting or alloying of bimetallic nanoparticles is a single-pulse process. Compared with the laser treated hetero nanoparticles shown in Figure 1 (ten laser pulses), the number of alloyed particles is significantly lower, although theoretically the entire volume of the particle solution is irradiated by the laser. This can be primarily explained by shadow effects and the energy profile of the laser beam. If several particles are arranged one behind the other parallel to the beam direction this leads to

 © 2023 The Authors. Particle & Particle Systems Characterization published by Wiley-VCH GmbH

15214117, 0, Downloaded from https://onlinelibrary.wiley.com/doi/10.1002/ppsc.202300021 by Cochrane Germany, Wiley Online Library on [13/07/2023]. See the Terms and Conditions (https://onlinelibrary.wiley.com/terms-and-conditions) on Wiley Online Library for rules of use; OA articles are governed by the applicable Creative Commons License

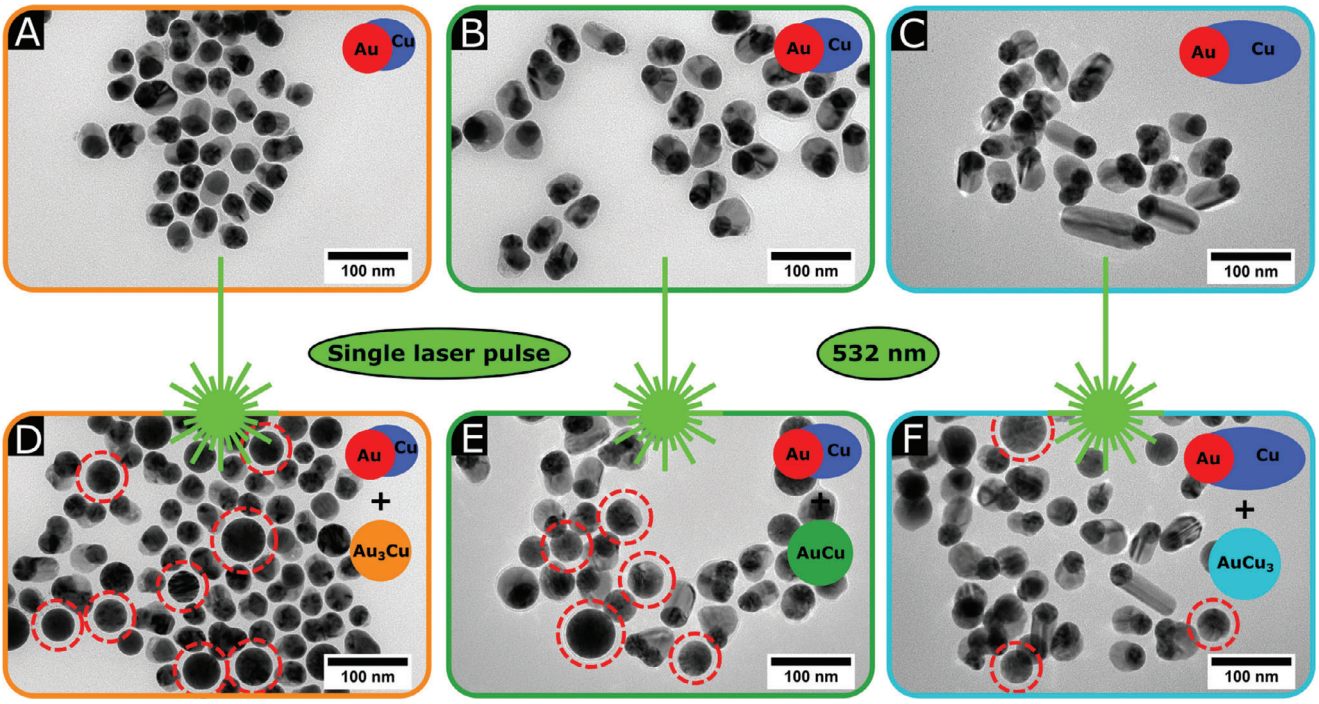

Figure 5. A–C) Single pulse experiments of the hetero nanoparticles. D–F) One single laser pulse led to the formation of nanoalloys, which shows that the laser-induced alloy formation is a one-pulse process (some alloyed particles are highlighted in red circles). The yield of nanoalloys can be increased by an increasing number of laser pulses.

shadow effects and an axial decrease in the laser fluence. In addition, the gaussian energy profile of the laser beam causes a lateral decrease of the laser fluence on the way from the center to edges of the beam. Regular mixing of the nanoparticle solution during the laser treatment is required to reduce the influence of these effects. Due to the need of certain amounts of nanoparticles for the characterization methods, it is also beneficial to find a balance between the concentration of the nanoparticle solution and the thickness of a suitable cuvette for the laser treatment. Depending on the gold to copper ratio (Figure 5A–C), the number of melted and alloyed particles after the laser treatment differs from each other. The yield of nanoalloys decreases with increasing copper domain size (Figure 5D–F), which in turn could also be related to shadowing effects and the energy profile of the laser beam as discussed above.

Finally, we also performed supporting X-ray photoelectron spectroscopy measurements (XPS), which are well in line with the proposed alloy formation (see Figures S9–S12 in the Supporting Information for a detailed discussion).

3. Conclusion

We separate the wet-chemical synthesis of hetero nanoparticles and the subsequent laser-induced alloy formation in two steps. This separation allows to combine the strengths of both methods, wet-chemical synthesis and plasmonic heating of colloidally dispersed nanoparticles without being limited by factors such as different redox potentials or required alloying temperatures. By varying the amount of copper precursor during the growth synthesis of copper domains on gold nanoparticles, Au–Cu hetero nanoparticles with different Au–Cu-ratio could be obtained. Subsequently, the hetero nanoparticles prepared in this way were irradiated with the second harmonic of a nanosecond Nd:YAG laser and heated up. This led to a fusion of the metal domains and the formation of Au–Cu nanoalloys. In TEM-EDX mappings, homogeneous distributed nanoalloys can be observed. The added-up volume of the metal domains also corresponds to the volume of the nanoalloys, which shows that the melting or alloying process is isochoric. In contrast to the alloying of the hetero nanoparticles, only a reshaping of the particles can be observed in the case of a simple mixture of gold and copper nanoparticles, indicating that a direct domain contact is required in the LML-alloying process presented here. In addition, single-pulse experiments demonstrated that an alloy formation is principally a single-pulse process and that an increase in the number of laser pulses only increases the yield of nanoalloys. Both, the Au–Cu hetero nanoparticles and the mixture of gold and copper nanoparticles were also investigated by energy dispersive X-ray spectroscopy (EDX), X-ray diffraction (XRD), UV–vis spectroscopy, and X-ray photoelectron spectroscopy (XPS) before and after the laser treatment. All techniques show that only in cases of the laser treatment of hetero nanoparticles with direct particle contact, nanoalloys were formed. The composition of the nanoalloys depends on the ratio of gold to copper in the respective hetero nanoparticles, which allows to control the composition of the final alloy during the wet-chemical synthesis of the hetero structures. In summary, the gold–copper-ratio of the hetero nanoparticles can be well tuned and controlled by wet-chemical synthesis. The subsequent laser-induced heating process leads to an isochoric melting and fusion of both metal

© 2023 The Authors. Particle & Particle Systems Characterization published by Wiley-VCH GmbH

15214117, 0, Downloaded from https://onlinelibrary.wiley.com/doi/10.1002/ppsc.202300021 by Cochrane Germany, Wiley Online Library on [13/07/2023]. See the Terms and Conditions (https://onlinelibrary.wiley.com/terms-and-conditions) on Wiley Online Library for rules of use; OA articles are governed by the applicable Creative Commons License

domains without changing the previous adjusted gold to copper ratio. Due to its simplicity, the separation of the well-tunable wet-chemical synthesis and the subsequent alloy formation via laser treatment directly in colloidal solution offers great potential for a variety of further multicomponent metal systems.

4. Experimental Section

Chemicals: Trisodium citrate dehydrate (99.0 %) was purchased from ABCR. Hydrogen tetrachloroaurate(III) trihydrate (99.99 %) was purchased from Alfa Aesar. Hexadecyltrimethylammonium bromide (CTAB, >99 %) was purchased from Acros Organics. Hexadecylamine (HDA, >95 %) was purchased from Merck. Copper(II) chloride (99%) was purchased from Sigma Aldrich. L-Ascorbic Acid was purchased from VWR.

Synthesis of Au Nanoparticles: Au nanoparticles were prepared in a seeded-growth synthesis according to the procedure described by Jia et al.[34] For the preparation of the seeds, 0.032 g (0.11 mmol, 2.2×10^{-3} M) trisodium citrate dihydrate were dissolved in 50 mL MilliQ water in a 100 mL three-neck flask. The solution was heated to the boiling point under stirring. After reaching the boiling point, 333 µL of a $HAuCl_4$ solution (25×10^{-3} M) was added. After 10 min, the temperature was set to 90 °C. For the growth of Au nanoparticles, 333 µL of trisodium citrate solution (60×10^{-3} M) was added followed by 333 µL of the $HAuCl_4$ solution (25×10^{-3} M) after two minutes. This step was 12 times repeated every 30 min. Then, the solution was cooled to room temperature. The Particles were separated by centrifugation (6000 g, 10 min), washed with water and redispersed in 5 mL of water.

Synthesis of Au–Cu Hetero Nanoparticles: Au–Cu hybrid nanoparticles were synthesized by a slightly modified procedure published by Jia et al.[34] First, 0.5 mL of the Au nanoparticle solution was separated by centrifugation (6000 g, 10 min) and redispersed in 0.5 mL CTAB solution (0.5×10^{-3} M). For the synthesis of Au–Cu hybrid nanoparticles, 12 mg (0.05 mmol) hexadecylamine was dissolved in 8.575 mL MilliQ water in a 25 mL three-neck flask. The solution was heated to the boiling point. After the hexadecylamine was completely dissolved, a certain amount of $CuCl_2$ solution (0.1 M) was added. In the case of the 3:1 ratio (Au:Cu) 30 µL, for the 1:1 ratio (Au:Cu) 100 µL and for the 1:3 ratio (Au:Cu) 300 µL $CuCl_2$ solution was used. After 15 min, the Au nanoparticles in CTAB solution followed by 825 µL ascorbic acid solution (0.2 M) were then added and stirred for 1 h under reflux. The solution was cooled to room temperature. The particles were separated by centrifugation (6000 g, 10 min), washed with water, and redispersed in 2 mL of water.

Synthesis of Cu Nanoparticles: The copper nanoparticles were prepared according to the Au–Cu hybrid nanoparticles with the exception that no gold particles were added. In contrast to the above-mentioned synthesis, only 75 µL $CuCl_2$ (0.1 M) solution was used in the case of monometallic copper nanoparticles.

Laser Treatment of Colloidally Dispersed Nanoparticles: The colloidally dispersed nanoparticles were irradiated in a quartz glass cuvette with the second harmonic of a Continuum Surelite I-10 nanosecond-pulsed Nd:YAG laser with a wavelength of 532 nm, a beam diameter of 6 mm and a pulse width of 6 ns. For this, 5 µL of the particle solution (50 µL in the case of XRD and XPS measurements) was dispersed in 500 µL of water in a special quartz glass cuvette. The dimensions of this cuvette are 1 cm × 1 cm × 3 cm (L×W×H). To reduce the volume of the cuvette, the cuvette was narrowed by two-thirds in one dimension by glass walls, resulting in two sides with different solution cross-sections. To achieve the highest possible irradiation efficiency, the cuvette was aligned accordingly with the larger irradiation cross-section to the laser beam. The particle was then irradiated with a laser fluence of 20 mJ cm^{-2} (incident laser fluence) for a total of 10 laser pulses. After each laser pulse, the cuvette was shaken. In this way, the influence of axial and lateral fluence gradients should be kept as low as possible.

XRD: The X-ray diffraction measurements were performed by a Bruker D8 Advance in reflection mode under the use of Cu Kα radiation (30 kV and 40 mA). Before and after laser treatment respectively, the nanoparticles were separated by centrifugation (6000 g, 5 min) and redispersed in 20 µL of water. The solution was then drop-casted onto a Si wafer and dried at air. Powder diffraction files from the ICSD database: Au: PDF no. 00-066-0091, Cu: PDF no. 00-004-0836, Au_3Cu: PDF no. 01-071-5023, AuCu: PDF no. 01-074-7033, $AuCu_3$: PDF no. 00-035-1357.

TEM: Transmission electron microscopy measurements were performed using a Fei Tecnai G2 F20 with a field emission gun operating at 200 kV. Before and after laser treatment respectively, the nanoparticles were separated by centrifugation (6000 g, 5 min) and redispersed in 20 µL of water. The nanoparticle solution was then drop-casted onto a Quantifoil carbon-coated copper grid (300 mesh) and dried at air.

Optical Spectroscopy (UV–vis-Spectroscopy: The UV–vis spectra were recorded with a modular spectrometer integrated into the laser setup. An Ocean Optics DH-2000 was used as the light source and an Ocean Optics HDX spectrometer as the detector. Both devices were connected to the cuvette holder, in which the cuvette was located, with a fiber optic cable. The light beam was perpendicular to the laser beam.

Supporting Information

Supporting Information is available from the Wiley Online Library or from the author.

Acknowledgements

D.K. would like to thank the Konrad-Adenauer-Stiftung (KAS) for financial support. D.D. and M.R. are grateful for funding by the German Research Foundation under Germany's Excellence Strategy within the Cluster of Excellence PhoenixD (EXC2122). P.B. acknowledge financial support by the Hannover School of Nanotechnology (HSN). D.D. and M.N. acknowledge financial support by the German Research Foundation (DGF) research grant 1580/5-1. The authors thank the Laboratory of Quantum and Nanoengineering for the use of the TEM and Apl. Prof. Armin Feldhoff for the use of the XRD.

Open access funding enabled and organized by Projekt DEAL.

Conflict of Interest

The authors declare no conflict of interest.

Data Availability Statement

The data that support the findings of this study are available in the supplementary material of this article.

Keywords

composition-control, hetero nanoparticles, laser melting in liquids (LML), nanoalloys

Received: February 6, 2023
Revised: April 14, 2023
Published online:

[1] H. Wang, A. Pyatenko, K. Kawaguchi, X. Li, Z. Swiatkowska-Warkocka, N. Koshizaki, *Angew. Chem., Int. Ed.* **2010**, *49*, 6361.
[2] a) M. Belekoukia, E. Kalamaras, J. Z. Tan, F. Vilela, S. Garcia, M. M. Maroto-Valer, J. Xuan, *Appl. Energy* **2019**, *247*, 517; b) H. Huang, L. V.

 © 2023 The Authors. Particle & Particle Systems Characterization published by Wiley-VCH GmbH

15214117, 0, Downloaded from https://onlinelibrary.wiley.com/doi/10.1002/ppsc.202300021 by Cochrane Germany, Wiley Online Library on [13/07/2023]. See the Terms and Conditions (https://onlinelibrary.wiley.com/terms-and-conditions) on Wiley Online Library for rules of use; OA articles are governed by the applicable Creative Commons License

Zhigilei, *J. Phys. Chem. C* **2021**, *125*, 13413; c) A. Plech, A. R. Ziefuß, M. Levantino, R. Streubel, S. Reich, S. Reichenberger, *ACS Photonics* **2022**, *9*, 2981; d) A. Takami, H. Kurita, S. Koda, *J. Phys. Chem. B* **1999**, *103*, 1226; e) S. Inasawa, M. Sugiyama, Y. Yamaguchi, *J. Phys. Chem. B* **2005**, *109*, 9404.

[3] S. Hashimoto, D. Werner, T. Uwada, *J. Photochem. Photobiol., C* **2012**, *13*, 28.

[4] a) A. Pyatenko, H. Wang, N. Koshizaki, T. Tsuji, *Laser Photonics Rev.* **2013**, *7*, 596; b) S. Malek, R. Poursalehi, *Sci. Iran., Trans. F* **2016**, *23*, 1489; c) H. Kurita, A. Takami, S. Koda, *Appl. Phys. Lett.* **1998**, *72*, 789.

[5] D. Zhang, B. Gökce, S. Barcikowski, *Chem. Rev.* **2017**, *117*, 3990.

[6] a) V. Amendola, D. Amans, Y. Ishikawa, N. Koshizaki, S. Scirè, G. Compagnini, S. Reichenberger, S. Barcikowski, *Chem. - Eur. J.* **2020**, *26*, 9206; b) G. W. Yang, *Prog. Mater. Sci.* **2007**, *52*, 648.

[7] a) S. Link, C. Burda, B. Nikoobakht, M. A. El-Sayed, *J. Phys. Chem. B* **2000**, *104*, 6152; b) S. Link, C. Burda, B. Nikoobakht, M. A. El-Sayed, *Chem. Phys. Lett.* **1999**, *315*, 12.

[8] D. Kranz, P. Bessel, M. Niemeyer, H. Borg, M. Rosebrock, R. Himstedt, N. C. Bigall, D. Dorfs, *J. Phys. Chem. C* **2022**, *126*, 15263.

[9] a) S. Itapu, D. G. Georgiev, P. Uprety, N. J. Podraza, *Phys. Status Solidi A* **2017**, *214*, 1600414; b) A. Voznyi, V. Kosyak, P. Onufrijevs, L. Grase, J. Vecstaudža, A. Opanasyuk, A. Medvid', *J. Alloys Compd.* **2016**, *688*, 130; c) P. Mitrev, G. Benvenuti, P. Hofman, A. Smirnov, N. Kaliteevskaya, R. Seisyan, *Tech. Phys. Lett.* **2005**, *31*, 908.

[10] a) J. N. Stanley, I. García-García, T. Perfrement, E. C. Lovell, T. W. Schmidt, J. Scott, R. Amal, *Chem. Eng. Sci.* **2019**, *194*, 94; b) S. Zhang, M. Li, J. Zhao, H. Wang, X. Zhu, J. Han, X. Liu, *Appl. Catal., B* **2019**, *252*, 24; c) C. Dwivedi, A. Chaudhary, S. Srinivasan, C. K. Nandi, *Colloid Interface Sci. Commun.* **2018**, *24*, 62; d) T. Li, G. Luo, K. Liu, X. Li, D. Sun, L. Xu, Y. Li, Y. Tang, *Adv. Funct. Mater.* **2018**, *28*, 1805828; e) L. Huang, J. Zou, J.-Y. Ye, Z.-Y. Zhou, Z. Lin, X. Kang, P. K. Jain, S. Chen, *Angew. Chem., Int. Ed.* **2019**, *58*, 8794.

[11] a) Y. Jin, F. Chen, J. Wang, *ACS Sustainable Chem. Eng.* **2020**, *8*, 2783; b) M. Walter, S. Doswald, M. V. Kovalenko, *J. Mater. Chem. A* **2016**, *4*, 7053.

[12] a) I. Darmadi, F. A. A. Nugroho, S. Kadkhodazadeh, J. B. Wagner, C. Langhammer, *ACS Sens.* **2019**, *4*, 1424; b) F. A. A. Nugroho, I. Darmadi, L. Cusinato, A. Susarrey-Arce, H. Schreuders, L. J. Bannenberg, A. B. Da Silva Fanta, S. Kadkhodazadeh, J. B. Wagner, T. J. Antosiewicz, A. Hellman, V. P. Zhdanov, B. Dam, C. Langhammer, *Nat. Mater.* **2019**, *18*, 489.

[13] a) Z. Wang, Y. Ju, S. Tong, H. Zhang, J. Lin, B. Wang, Y. Hou, *Nanoscale Horiz.* **2018**, *3*, 624; b) X. Ye, X. He, Y. Lei, J. Tang, Y. Yu, H. Shi, K. Wang, *Chem. Commun.* **2019**, *55*, 2321; c) E. Girgis, W. K. B. Khalil, A. N. Emam, M. B. Mohamed, K. V. Rao, *Chem. Res. Toxicol.* **2012**, *25*, 1086.

[14] S. Thota, Y. Wang, J. Zhao, *Mater. Chem. Front.* **2018**, *2*, 1074.

[15] P. Lu, J. Zhou, Y. Hu, J. Yin, Y. Wang, J. Yu, Y. Ma, Z. Zhu, Z. Zeng, Z. Fan, *J. Mater. Chem. A* **2021**, *9*, 19025.

[16] a) K.-H. Huynh, X.-H. Pham, J. Kim, S. H. Lee, H. Chang, W.-Y. Rho, B.-H. Jun, *Int. J. Mol. Sci.* **2020**, *21*, 5174; b) J. Zhang, Y. Yu, B. Zhang, *Phys. Sci. Rev.* **2020**, *5*, 1; c) R. Ferrando, J. Jellinek, R. L. Johnston, *Chem. Rev.* **2008**, *108*, 845.

[17] a) N. E. Motl, E. Ewusi-Annan, I. T. Sines, L. Jensen, R. E. Schaak, *J. Phys. Chem. C* **2010**, *114*, 19263; b) A. K. Sra, R. E. Schaak, *J. Am. Chem. Soc.* **2004**, *126*, 6667; c) R. E. Schaak, A. K. Sra, B. M. Leonard, R. E. Cable, J. C. Bauer, Y.-F. Han, J. Means, W. Teizer, Y. Vasquez, E. S. Funck, *J. Am. Chem. Soc.* **2005**, *127*, 3506.

[18] H. Prunier, J. Nelayah, C. Ricolleau, G. Wang, S. Nowak, A.-F. Lamic-Humblot, D. Alloyeau, *Phys. Chem. Chem. Phys.* **2015**, *17*, 28339.

[19] a) B. Pauwels, G. van Tendeloo, E. Zhurkin, M. Hou, G. Verschoren, L. Theil Kuhn, W. Bouwen, P. Lievens, *Phys. Rev. B* **2001**, *63*, 165406; b) S. Sebastian, C. L. Linslal, C. Vallbhan, V. Nampoori, P. Radhakrishnan, M. Kailasnath, *Solid State Commun.* **2015**, *628*, 25; c) J. Simon, V. Nampoori, M. Kailasnath, *Optik* **2019**, *195*, 163168; d) S. Besner, M. Meunier, *J. Phys. Chem. C* **2010**, *114*, 10403; e) N. G. Semaltianos, R. Chassagnon, V. Moutarlier, V. Blondeau-Patissier, M. Assoul, G. Monteil, *Nanotechnology* **2017**, *28*, 155703.

[20] A. Basagni, V. Torresan, P. Marzola, M. B. van Fernàndez Raap, L. Nodari, V. Amendola, *Faraday Discuss.* **2023**, *242*, 286.

[21] R. Kuladeep, L. Jyothi, K. S. Alee, K. L. N. Deepak, D. N. Rao, *Opt. Mater. Express* **2012**, *2*, 161.

[22] G. Compagnini, E. Messina, O. Puglisi, V. Nicolosi, *Appl. Surf. Sci.* **2007**, *254*, 1007.

[23] G. González-Rubio, P. Díaz-Núñez, W. Albrecht, V. Manzaneda-González, L. Bañares, A. Rivera, L. M. Liz-Marzán, O. Peña-Rodríguez, S. Bals, A. Guerrero-Martínez, *Adv. Opt. Mater.* **2021**, *9*, 2002134.

[24] J. E. S. van der Hoeven, T. A. J. Welling, T. A. G. Silva, J. E. van den Reijen, C. L. Fontaine, X. Carrier, C. Louis, A. van Blaaderen, P. E. de Jongh, *ACS Nano* **2018**, *12*, 8467.

[25] R. Fathima, A. Mujeeb, *Mater. Res. Express* **2018**, *5*, 125011.

[26] T. R. Machado, N. G. Macedo, M. Assis, C. Doñate-Buendia, G. Mínguez-Vega, M. M. Teixeira, C. C. Foggi, C. E. Vergani, H. Beltrán-Mir, J. Andrés, E. Cordoncillo, E. Longo, *ACS Omega* **2018**, *3*, 9880.

[27] F. Hajiesmaeilbaigi, M. Fazeli Jadidi, A. Motamedi, *Acta Phys. Pol. A* **2012**, *121*, 59.

[28] M. Watanabe, H. Takamura, H. Sugai, *Nanoscale Res. Lett.* **2009**, *4*, 565.

[29] a) K. A. Kane, A. C. Reber, S. N. Khanna, M. F. Bertino, *Prog. Nat. Sci.: Mater. Int.* **2018**, *28*, 456; b) J. Wang, L. Guo, B. Pan, T. Jin, Z. Li, Q. Tang, P. Andreazza, Y. Chen, L. An, F. Chen, *Faraday Discuss.* **2023**, *242*, 499.

[30] A. Pyatenko, H. Wang, N. Koshizaki, *J. Phys. Chem. C* **2014**, *118*, 4495.

[31] T. Tsuji, T. Yahata, M. Yasutomo, K. Igawa, M. Tsuji, Y. Ishikawa, N. Koshizaki, *Phys. Chem. Chem. Phys.* **2013**, *15*, 3099.

[32] D. Hong, A. Sharma, D. Jiang, E. Stellino, T. Ishiyama, P. Postorino, E. Placidi, Y. Kon, K. Koga, *ACS Omega* **2022**, *7*, 31260.

[33] a) A. R. Denton, Ashcroft N. W., *Phys. Rev. A* **1991**, *43*, 3161; b) F. Gonella, G. Mattei, P. Mazzoldi, C. Sada, G. Battaglin, E. Cattaruzza, *Appl. Phys. Lett.* **1999**, *75*, 55.

[34] H. Jia, Y. Yang, T. H. Chow, H. Zhang, X. Liu, J. Wang, C. Zhang, *Adv. Funct. Mater.* **2021**, *31*, 2101255.

© 2023 The Authors. Particle & Particle Systems Characterization published by Wiley-VCH GmbH

15214117, 0, Downloaded from https://onlinelibrary.wiley.com/doi/10.1002/ppsc.202300021 by Cochrane Germany, Wiley Online Library on [13/07/2023]. See the Terms and Conditions (https://onlinelibrary.wiley.com/terms-and-conditions) on Wiley Online Library for rules of use; OA articles are governed by the applicable Creative Commons License